



**HAL**  
open science

## Impact of oxygen contamination on the electrochemical impedance spectroscopy of iron corrosion in H<sub>2</sub>S solutions

Martien Duvall Deffo Ayagou, Gaurav R. Joshi, Thi Tuyet Mai Tran, Bernard Tribollet, Eliane Sutter, Christophe Mendibide, Claude Duret-Thual, Jean Kittel

### ► To cite this version:

Martien Duvall Deffo Ayagou, Gaurav R. Joshi, Thi Tuyet Mai Tran, Bernard Tribollet, Eliane Sutter, et al.. Impact of oxygen contamination on the electrochemical impedance spectroscopy of iron corrosion in H<sub>2</sub>S solutions. *Corrosion Science*, 2020, 164, pp.108302. 10.1016/j.corsci.2019.108302 . hal-02468028

**HAL Id: hal-02468028**

**<https://ifp.hal.science/hal-02468028>**

Submitted on 5 Feb 2020

**HAL** is a multi-disciplinary open access archive for the deposit and dissemination of scientific research documents, whether they are published or not. The documents may come from teaching and research institutions in France or abroad, or from public or private research centers.

L'archive ouverte pluridisciplinaire **HAL**, est destinée au dépôt et à la diffusion de documents scientifiques de niveau recherche, publiés ou non, émanant des établissements d'enseignement et de recherche français ou étrangers, des laboratoires publics ou privés.

## **Impact of oxygen contamination on the electrochemical impedance spectroscopy of iron corrosion in H<sub>2</sub>S solutions**

Martien Duvall Deffo Ayagou<sup>1,2</sup>, Gaurav R. Joshi<sup>1</sup>, Thi Tuyet Mai Tran<sup>3</sup>, Bernard Tribollet<sup>3</sup>, Eliane Sutter<sup>3</sup>, Christophe Mendibide<sup>2</sup>, Claude Duret-Thual<sup>2</sup>, Jean Kittel<sup>1\*</sup>.

*1- IFP Energies nouvelles, Rond-Point de l'échangeur de Solaize ,BP3, 69360 Solaize, France*

*2- Institut de la Corrosion – Site de Saint-Etienne, zone d'activités du parc secteur Gampille 42490 Fraisses, France*

*3- Sorbonne Université, CNRS, Laboratoire Interfaces et Systèmes Electrochimiques (LISE), F-75005 Paris, France*

\* corresponding author: [jean.kittel@ifpen.fr](mailto:jean.kittel@ifpen.fr)

### **Abstract**

Oxygen pollution in hydrogen sulfide (H<sub>2</sub>S) saturated test solutions can compromise the results of standardized tests, which guide materials selection in safety-critical components. To examine the temporal evolution of such contamination, we have used the electrochemical methods of impedance spectroscopy and hydrogen permeation to study the corrosion of iron exposed to oxygen-polluted H<sub>2</sub>S-saturated solutions. EIS analyses were performed with a previously developed model, which

explicitly accounts for the contribution of a conductive and porous iron sulfide overlayer. A good correlation is found between corrosion estimates from EIS and weight loss, measured to be higher than the O<sub>2</sub>-free case. Hydrogen permeation studies across the iron membrane were conducted to qualitatively evaluate the impact of dissolved O<sub>2</sub> on hydrogen entry. We observe that O<sub>2</sub> contamination was found to significantly reduce hydrogen charging into the metal.

**keywords** : Corrosion; iron; oxygen; H<sub>2</sub>S; EIS

## 1. Introduction

In oil and gas environments, dissolved CO<sub>2</sub> and H<sub>2</sub>S are the main corrosive agents, present in varying proportions, co-produced with hydrocarbon fluids. Low alloy steel assets are prone to degradation through corrosion and stress-cracking issues [1], including those caused by the diffusion of hydrogen into the metal. Over the years, the oil and gas sector has gained considerable experience in the management of corrosion of low alloy steels in acid media containing H<sub>2</sub>S. Since O<sub>2</sub> is often absent from these production environments, laboratory studies almost exclusively concern O<sub>2</sub>-free environments. During standardized tests that are used in the quality control and selection of steels for use in H<sub>2</sub>S environments, continuous oxygen contamination at a low concentration is always possible if control practices are not well regulated. Previous work indicates that O<sub>2</sub> ingress modifies the solution chemistry, the mechanisms and nature of the corrosion deposits, as well as the hydrogen uptake [2–6], which may affect final materials testing results in

standardized and fitness for purpose tests. Indeed, in the field, O<sub>2</sub> contamination may still arise, for instance from storage tanks of injected chemicals, during gas-lift, or from process equipment such as pumps.

In the study of the evolution of H<sub>2</sub>S corrosion reactions as a function of time, electrochemical impedance spectroscopy (EIS) is shown to be a suitable and effective measurement technique [2,7]. We have previously characterized the EIS response of pure iron in 35 g L<sup>-1</sup> NaCl solutions saturated with 1 bar H<sub>2</sub>S at ambient temperature with dissolved oxygen concentrations ([O<sub>2</sub>]<sub>aq</sub>) lower than 10 parts per billion by weight (ppb) [2]. The proposed equivalent circuit model accounts for the porous, and conductive, nature of the changing iron sulfide overlayer. The broad trends of the impact of oxygen contamination on the corrosion performance of iron were presented in reference [6]. That article, however, lacked a detailed discussion regarding the specific observations on the effect of oxygen contamination on the evolution of the resulting electrochemical impedance data. Evaluating these O<sub>2</sub>-polluted corrosion kinetics data of Fe in H<sub>2</sub>S-saturated solution, with respect to the O<sub>2</sub>-free condition, is valuable work that may help to understand the particularities of measuring high surface corrosion rates with low uptake of hydrogen [6]. Principally, we believe that interesting aspects about the nature of the corrosion product film and its evolution could be revealed through the analysis of EIS results. Therefore, we extend that investigation here by probing the iron interface using EIS in the same H<sub>2</sub>S-saturated solution, although contaminated with a fixed concentration of dissolved oxygen. To be precise, the O<sub>2</sub> concentration limit given in the standard NACE TM0177 is 50 ppb [8], but to exacerbate the consequences of O<sub>2</sub> contamination we conduct our experiments under an O<sub>2</sub> partial pressure corresponding to [O<sub>2</sub>]<sub>aq</sub> = 500

ppb. The AC impedance data are collected as a function of time over few weeks to represent the typical time-scale of sulfide stress cracking (SSC) qualification tests.

## 2. Experimental procedure

The preparation and experimental procedures for corrosion and hydrogen permeation testing are detailed in Ref. [2]. We have used a Devanathan-Stachurski type double chamber cell, with the high purity iron membrane clamped in-between as the two-sided working electrode, that permits the acquisition of EIS measurements on the hydrogen charging side and hydrogen permeation measurements at the Pd-coated exit side (in deaerated 0.1 M NaOH) – as long as the correct electronics precautions are taken (i.e. avoiding ground loops). Platinum counter electrodes were used in both cells. An Ag/AgCl electrode in a liquid salt bridge was used as the reference electrode in the O<sub>2</sub>-polluted H<sub>2</sub>S-saturated medium (during EIS measurements), whereas an Hg/HgO electrode was employed in the H-detection cell (during H-permeation measurements). Since the aim in the present study was to examine the effect of O<sub>2</sub> contamination on the EIS response of the iron surface exposed to the H<sub>2</sub>S medium, we continuously impose an oxygen partial pressure of 13 mbar in the gas stream, which corresponds to an [O<sub>2</sub>]<sub>aq</sub> = 500 ppb in the test solution (35 g L<sup>-1</sup> NaCl, T = 24°C) at equilibrium. After initial deaeration of the solution in a preparation flask by argon (18 h), it was purged with a gas mixture of H<sub>2</sub>S (87.5%), N<sub>2</sub> (11.25%) and O<sub>2</sub> (1.25%) for a period of 6 h. After transferring the solution to the 'H-charging' cell, the same gas mixture was bubbled through the test solution to sustain the oxygen contamination over the 3-4 week experiment duration. Experimental outputs include 1) continuous in-situ pH measurement and periodic sampling of the test solution for ionic chromatography analysis; 2) pure iron coupon

weight-loss and SEM analyses; 3) anodic extraction of hydrogen permeation at the H-exit face of the membrane, and 4) EIS at the H-entry face of the membrane – i.e. the key results of discussion in the current article. The potentiostatic EIS measurements were conducted with a polarisation of  $\pm 10$  mV amplitude vs. open circuit potential, ranging from 10 kHz to 1 mHz, where each iteration was followed by 2 hours rest at the electrode's open circuit potential.

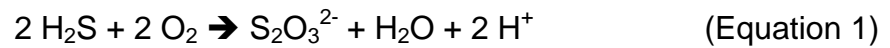
### **3. Results and discussion**

#### **3.1. Impact of O<sub>2</sub> on test solution chemistry**

In a previous article, we have discussed how changes to the test solution chemistry take place (changes to pH) in both O<sub>2</sub>-free and O<sub>2</sub>-polluted systems [6]. In the very early stages of iron corrosion, the bulk solution pH is measured to increase as a result of the release of alkalinity (HS<sup>-</sup><sub>(aq)</sub>) during cathodic reduction at iron surfaces. The subsequent saturation of the test solution with iron sulfide stabilizes the bulk solution pH until the end of the test as shown in Fig. 1. On the contrary, with O<sub>2</sub> contamination, a continuous decrease of pH is observed, from pH = 4.3 (FeS saturation pH) after few days and down to pH = 3.1 after 3 weeks exposure.

Ionic chromatography (IC) analyses of solution samples taken from different time exposures confirm that sulfates (SO<sub>4</sub><sup>2-</sup>) were the main, stable species formed, as a result of dissolved O<sub>2</sub> – H<sub>2</sub>S reactions over time. Their concentration increased linearly with exposure time in the presence of continuous O<sub>2</sub> ingress, whereas they stayed at minute levels in the reference O<sub>2</sub>-free conditions. According to the

literature, reaction paths leading to sulfate involve an intermediate step with thiosulfate ( $\text{S}_2\text{O}_3^{2-}$ ) formation accompanied by the release of  $\text{H}^+$  [3,4] :



The more stable sulfate species may then be formed by various paths, e.g. by direct oxidation:



Apart from direct oxidation, thiosulfate is also known to enhance iron and steel corrosion, with additional intermediate reactions involving  $\text{H}_2\text{S}$  and elemental sulfur formation [7,9]. The temporal evolution of the measured concentrations (mg/L) of the important species in solution is presented in Fig 1. Dissolved  $\text{H}_2\text{S}$  remains the species in excess, on the order of 2 – 3 g/L.

*Fig. 1: The evolution of the bulk solution concentrations of  $\text{H}^+$  (from pH measurements) and primary identified aqueous  $\text{H}_2\text{S}$ - $\text{O}_2$  reaction anion products of sulfites, thiosulfates and sulfates in  $35 \text{ g L}^{-1}$  NaCl solution saturated with 1 bar  $\text{H}_2\text{S}$  at 24 °C in (a)  $\text{O}_2$ -free and (b)  $\text{O}_2$ -polluted solution as a function of time. These data are reproduced from ref. [6].*

### 3.2. Impact of O<sub>2</sub> on EIS data

As a direct consequence of the changes of test solution chemistry imparted by oxygen, the electrochemical behavior of the iron membranes is observed to differ. Fig. 2 presents the evolution of the open circuit potentials (OCP) as a function of time. In the absence of O<sub>2</sub>, the OCP of pure iron remains steady at a value of approximately -690 mV<sub>Ag/AgCl</sub> over the course of the 3-4 week long experiment (much like the pH). For the O<sub>2</sub>-polluted test, the OCP is comparable to the O<sub>2</sub>-free test during the early stages, but then increases as the test solution pH decreases. At the end of the test, the rise in OCP is approximately +30 mV. It is noted how the rise of OCP correlates with the rising [H<sup>+</sup>]<sub>aq</sub> in Fig 1(b) and therefore the oxidizing power of the solution, as predicted by Evans Theory. Indeed, this theory shows that an observation of a simultaneous increase in OCP (and measured corrosion current density ( $I_{\text{corr}}$ ) – see later) can be strongly associated with an increase in the cathodic reduction current density as a result of the higher oxidant concentration/activity in the test medium. In this case, we assume that the anodic iron dissolution kinetics reaction slope remains unchanged and suggest that increasing rates of metal loss ( $I_{\text{corr}}$ ) in the O<sub>2</sub>-contaminated solution (see later) is driven by the rising kinetics of cathodic proton reduction.

*Fig. 2: The evolution of open circuit potentials of Fe in 35 g L<sup>-1</sup> NaCl solution saturated with 1 bar H<sub>2</sub>S at 24 °C, with (red) and without (black) oxygen contamination.*

Impedance diagrams measured at short immersion times (2 hours) in test solutions with and without oxygen contamination are presented in Fig. 3. These diagrams present similar shapes and frequency distributions, with two capacitive loops. According to Ma and co-workers, these impedance diagrams correspond to the anodic dissolution of iron with an intermediate step involving some type of adsorbed species [10,11]. As these authors do, we also hesitate to describe the exact nature of the adsorbed species here since the mechanism of corrosion including the formation of iron sulfides is complicated and remains contested. The equivalent circuit adopting this general principle is given in Fig. 4. In this circuit,  $R_t$  is the charge transfer resistance associated with the double layer capacitance  $CPE_{dl}$ , and  $R_a$  and  $CPE_a$  are associated with the adsorption – desorption steps of anodic iron dissolution. Constant phase elements (CPE) are used instead of pure capacitance due to the to time constant distribution associated with surface heterogeneities. Consequently, the charge transfer corresponding to the corrosion reaction is represented by the diameter of the high frequency semi-circle, and it is not significantly modified by oxygen contamination at short exposure times.

*Fig. 3: Nyquist diagrams of pure iron measured after 2 hours exposure in 35 g L<sup>-1</sup> NaCl saturated with 1 bar H<sub>2</sub>S at 24°C for a) O<sub>2</sub>-free and b) O<sub>2</sub>-contaminated solutions*

*Fig. 4: Equivalent circuit for the corrosion of pure iron in H<sub>2</sub>S containing environment at short exposure times [10,11].*

At longer exposure times, however, the shape of the impedance diagrams changes quite dramatically, with significant differences observed depending on whether oxygen contamination is involved or not. The Nyquist diagrams at different time intervals are presented in Fig. 5(a) and (b) for tests without and with oxygen contamination respectively. Under O<sub>2</sub> contamination (Fig 5(b)), we observe a completely different impedance evolution. After long immersion times, a decrease of the second capacitive loop is observed, to the extent that it is no longer apparent. Here, the Nyquist diagram may be described as an overlap of two capacitive arcs. This trend is quite different to data obtained after similar long exposures, without O<sub>2</sub> ingress, as shown in Fig. 5(a).

*Fig. 5 : Nyquist diagrams of pure iron exposed to 35 g L<sup>-1</sup> NaCl saturated with 1 bar H<sub>2</sub>S at 24°C for a) O<sub>2</sub>-free and b) O<sub>2</sub>-contaminated solutions at various exposure times (orthonormal representation with translation of the y-axis as exposure time increases).*

Kramers-Kronig transformations were used to validate all the raw EIS experimental data. Moreover, high-frequency measurements validity had to be checked. Indeed, at high frequency, the impedance of the system is so small that the noise of the measurement device significantly impairs the quality of the result. Considering that the impedance of the system in the high frequency domain can be approximated by the electrolyte resistance (R<sub>e</sub>) in series with the high frequency capacitance (C<sub>HF</sub>),

and taking into account a measurement noise of 1%, one easily determines that all the impedance values for which  $1/\omega C_{HF}$  is lower than 1% of  $R_e$  cannot be trusted. As  $C_{HF}$  is close to  $50 \text{ mF cm}^{-2}$  at the beginning of the tests, and  $R_e$  is in the range of  $6 \Omega$  during our experiments, the maximum frequency above which the data become unreliable is in the range of 50 Hz, a value that further decreases with exposure time.

We have analyzed the EIS data of the  $O_2$ -free system in detail elsewhere [2]. There, it was discussed that the evolution of impedance diagrams appears to be influenced by the formation of a highly porous and conductive iron sulfide layer. A new impedance model was developed, and is presented in Fig. 6. This model includes the contribution of the porous film ( $Z_{film}$ ) in parallel with the impedance of Fig. 4. In this model, the double layer capacitance ( $C_{dl}$ ) is placed across the entire film because of the very low band gap/metallic conductivity of FeS mackinawite [12]. Huang *et al* applied the ion selectivity technique across mackinawite to conclude that it displays an n-type semiconductive nature [13]. It implies, possibly due to the slight sulfur ion deficiency in mackinawite, that electron charge is transferred through the FeS structure's conduction band. Elsewhere, Tjelta *et al* conducted cathodic reaction electrochemical studies on mackinawite electrodes and reported that the Tafel slopes obtained were quite comparable to those from bare steel electrodes [14], which justifies our choice of how  $C_{dl}$  is presented in the model.

The behavior of the film was modeled according to the work of de Levie, who showed that the impedance of porous electrode could be written as [15]:

$$Z_{film,porous} = \sqrt{\rho Z_{eq}} / \sqrt{2n\pi r}^{3/2} \quad (\text{Equation 3})$$

In this expression,  $Z_{eq}$  defines the interfacial impedance at the surface of the conductive film inside the pores, and  $n$ ,  $r$  and  $\rho$  are respectively the number of pores, their radii and the resistivity of the electrolyte. The square root term of the porous electrode contribution explains the  $45^\circ$  inclination of the impedance at long exposure times observed in pure  $H_2S$  without  $O_2$  contamination, suggesting an increasing contribution of the porosity of the film.

*Fig. 6: Equivalent circuit for the corrosion of pure iron in  $H_2S$  containing environment with the formation of a conductive and porous  $FeS$  layer [2].*

According to the interpretations of the equivalent circuit model in Fig. 6, the changes to the EIS data measured under  $O_2$  contamination appear to mainly affect the contribution of the iron sulfide layer ( $Z_{film}$ ), i.e. the low frequency tail. Since very weak or negligible porous film responses were measured in the impedance diagrams obtained in  $O_2$ -contaminated solutions at exposure times beyond 200 h (i.e. the lack of a linear tail in Nyquist data), the analysis of these test results was carried out with the nested equivalent circuit model of Fig. 4. Here, we have obtained a good correlation between fitted impedance and experimental data (Fig. 7). The values of model parameters corresponding to these fitted impedances are gathered in Table 1. Brug's relationship has been used to derive the effective double layer capacitance from the CPE (constant phase elements) [16,17]:

$$C_{dl} = Q^{\frac{1}{\alpha}} (R_e^{-1} + R_t^{-1})^{\frac{\alpha-1}{\alpha}} \quad (\text{Equation 4})$$

*Fig. 7: Comparisons between experimental (open symbols) and fitted impedance (lines) measured after 2 h (a), 47 h (b) and 572 h (c) exposure in O<sub>2</sub>-contaminated solutions, using the equivalent circuit of Fig. 4.*

*Table 1: Component values of equivalent circuit of Figure 4 giving the best fit of experimental impedance in O<sub>2</sub> contaminated solution at various exposure times.*

These differences in impedance data suggest that the morphology of the corrosion product layer is likely quite different. This is confirmed by SEM observation of cross-sections of pure iron specimens after 700 hours exposure with and without O<sub>2</sub> contamination (Fig. 8). Compared to the dense and porous layer of 20 to 30 μm thickness FeS formed under O<sub>2</sub>-free conditions, the overlayer formed in the O<sub>2</sub>-polluted medium possesses no micro-porosity at this resolution, and is loosely adhered to the underlying Fe substrate. Such morphologies of FeS films on pure iron substrate are quite representative of the Fe surfaces from O<sub>2</sub>-free/O<sub>2</sub>-contaminated systems in this work. It was generally noted that a far less homogeneous overlayer comprising iron sulfide/s forms in the presence of O<sub>2</sub> contamination [6].

*Fig. 8: Cross-sectional SEM images of pure iron after exposure to 35 g L<sup>-1</sup> NaCl saturated with 1 bar H<sub>2</sub>S at 24°C in a) O<sub>2</sub>-polluted and b) O<sub>2</sub>-free solution.*

*Fig. 9: Evolution of charge transfer resistance ( $R_t$  from EIS modeling) with and without oxygen contamination.*

The evolution of charge transfer resistance as a function of exposure time is shown in Fig. 9 for the experiments conducted with and without O<sub>2</sub> contamination. During the early hours of exposure,  $R_t$  present similar evolution in both experiments and start at values near 250 Ω.cm<sup>2</sup> after a few hours, reaching a plateau at 350 – 400 Ω.cm<sup>2</sup> between 24 hours and 100 hours. Whereas  $R_t$  in O<sub>2</sub>-free condition remain consistent over the remaining 3 weeks, those in the O<sub>2</sub>-polluted system are observed to decrease after 150 hours exposure, and at an even faster rate beyond the 350<sup>th</sup> hour. This drop generally correlates well with the measured decrease in bulk solution pH. It suggests that the effect of O<sub>2</sub> contamination is not immediate but rather presents itself over time in a cumulative manner. We believe that the poor interfacial coverage of the overlayer (that normally affords some protection) as well as the participation of additional chemical and cathodic electrochemical reactions from the rising concentrations of the products of the O<sub>2</sub> and H<sub>2</sub>S reaction, i.e. sulfites, thiosulfates and elemental sulfur, result in the increasing Fe corrosion rate trend in O<sub>2</sub>-polluted H<sub>2</sub>S solutions [6].

After 600 hours exposure,  $R_t$  is as low as  $100 \Omega \cdot \text{cm}^2$  under  $\text{O}_2$  contamination, although still greater than  $400 \Omega \cdot \text{cm}^2$  in the conditions devoid of  $\text{O}_2$  entry. Since the corrosion rate is inversely proportional to  $R_t$ , one could expect a 4-fold increase of instantaneous corrosion rate after 600 hours exposure in the  $\text{O}_2$ -contaminated system. From EIS analysis, corrosion current densities ( $J_{corr}$ ) were calculated from  $R_t$  using the Stern and Geary relationship with an anodic Tafel coefficient ( $b_a$ ) of 40 mV/decade, as expected in  $\text{H}_2\text{S}$  environments [18]:

$$J_{corr} = b_a / 2.3R_t \quad (\text{Equation 5})$$

We note that for both tests, an excellent agreement was found between the average corrosion rates calculated from EIS measurements (530  $\mu\text{m}/\text{year}$  and 854  $\mu\text{m}/\text{year}$  without and with  $\text{O}_2$ ) and weight-loss analysis of coupons (489  $\mu\text{m}/\text{year}$  and 976  $\mu\text{m}/\text{year}$  without and with  $\text{O}_2$ ). We demonstrate, therefore, that the agreement between weight loss and electrochemical corrosion calculations justifies the validity and applicability of the nested equivalent circuit impedance model used (Fig. 4) in the present study.

The evolution of the double layer capacitance with time is presented in Fig. 10. Under both conditions (with and without oxygen), an increase in the capacitance with time is initially observed that we attribute to the surface area increase of the iron sulfide layer. At this early stage, the FeS film does not behave as a porous electrode with a  $45^\circ$  inclination, but only as a plane electrode with a large conductive area, which explain the unexpectedly high values of  $C_{dl}$ . As the crystalline mackinawite

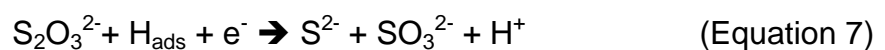
agglomeration continues, the film grows in surface area and porosity. The rising interfacial area means an increasing amount of charge distribution at the interface and so the effective double layer capacitance continues to increase. Abrupt breaks in the evolution of the capacitance are also observed at certain times, which are interpreted to be strain-induced delamination events of the iron sulfide layer during its growth [19]. In addition, under O<sub>2</sub> contamination, there is a minor stabilization, and a decrease in the capacitance towards the end of the test. The maximum capacitance in the presence of dissolved oxygen reaches approximately 22 mF/cm<sup>2</sup>, which is a value that is approximately 3 times lower than the maximum capacitance obtained in O<sub>2</sub>-free tests. Such lower capacitance could be a result of the test medium acidification that would limit the continuous formation (rising surface area) of a porous iron sulfide overlayer and favor the dissolution of the already existing layer. Indeed, this is supported by the cross-sectional analysis of the Fe sample in O<sub>2</sub>-polluted H<sub>2</sub>S solution, which portrays a patchy, poorly adherent iron sulfide (Fig. 8).

*Fig. 10: Evolution of double layer capacitance ( $C_{dl}$  from EIS modeling) with and without oxygen contamination.*

### **3.3. Impact of O<sub>2</sub> on hydrogen uptake**

In the previous article related to impedance behavior without oxygen contamination, we have shown that the corrosion current density and hydrogen permeation current density were similar during the total exposure time, resulting in a permeation efficiency close to 100% [2]. Here, we make the same comparison for the oxygen-

contaminated case. The results are presented in Fig. 11. It is seen that the influence of oxygen increases with time: at short exposures, until approximately 120 hours, the trends are similar with and without O<sub>2</sub>, although permeation current densities are slightly lower in the former situation. Beyond this 120 hour- threshold, the increasing corrosion current density and the decreasing hydrogen permeation density continuously deviate. As a consequence, the permeation efficiency, defined as the ratio between  $J_{perm}$  and  $J_{corr}$ , suffers a continuous drop and reaches a value as low as 20% after 600 hours exposure. Despite obtaining a less protective film that will permit a greater fraction of the Fe surface exposed to the corrosive H<sub>2</sub>S solution, these electrochemical data suggest that certain phenomena drive intense iron corrosion from a non-hydrogenating source. The reactants for such processes are quite possibly supplied from the H<sub>2</sub>S – O<sub>2</sub> reaction products, since their concentration keeps increasing in the limited volume reactor vessel over time. For instance, thiosulfate is recognized as a candidate for direct cathodic reduction, either directly as an oxidizing agent, or in combination with atomic hydrogen already present at the surface of the electrode [20]:



In this latter case, thiosulfate reduction may play a detrimental role in hydrogen uptake into the metal, as it reacts with the intermediate species H<sub>ads</sub>. Then, the EIS corrosion current density is increased without hydrogen charging.

*Fig. 11: Comparison of  $J_{perm}$  with  $J_{corr}$  determined from  $R_t$  values from EIS fittings for the tests without (a) and with (b)  $O_2$  contamination.*

### 3.4. Technological impact and relevance

Electrochemical impedance spectroscopy is a sensitive and powerful technique that differentiates, with a lot of detail, the electrochemical reaction kinetics of Fe in the  $O_2$ -free and  $O_2$ -polluted  $H_2S$ -saturated solution. Quite elegantly, and *in situ*, it demonstrates how the oxygen contaminated system disrupts the development of a highly porous FeS electrode surface. Understanding how the  $O_2$ -polluted corrosion kinetics data of Fe in  $H_2S$ -saturated solution evolve over time, with respect to the  $O_2$ -free condition, is a valuable effort that reveals high surface corrosion rates with a decreasing uptake of atomic hydrogen. Such a phenomenon could present doubt in the results of fitness for purpose or standardized tests for ferritic materials in sour environments. For instance, the changes in solution chemistry resulting from  $O_2$  ingress could modify the way a strained steel alloy fails, going from cathodic hydrogen-entry driven fracture ( $O_2$ -free) to one dominated by an anodic dissolution/localised corrosion induced stress corrosion cracking ( $O_2$ -polluted). Conversely, the less hydrogenating " $O_2$ -contaminated" solution may limit hydrogen uptake to the extent that a material "passes", and be deemed suitable for a critical application that is far more severe than the imposed lab conditions. Here, the consequences for safe operation might be disastrous. Elsewhere, considering that the aeration treatments may be used in the geothermal and biogas production sectors as a means of decreasing the dissolved  $H_2S$  concentration [24,25], the

results of the current article present the nature and kinetics of the corrosive degradation of an exposed low alloy steel component as a result of the products of the  $\text{H}_2\text{S-O}_2$  reaction chemistry (e.g. increased acidity and thiosulfates).

#### 4. Conclusions

The corrosion of pure iron in oxygen-contaminated  $\text{H}_2\text{S}$ -saturated 35 g/L NaCl ( $T = 24^\circ\text{C}$ ,  $\text{pH}_{\text{start}} = 3.9$ ) was studied using electrochemical impedance spectroscopy over 3 – 4 weeks. An impedance model developed in a previous article was found to satisfactorily fit the experimental data, and extract the relevant parameters associated with the dynamic interfacial processes. It was shown that  $\text{O}_2$  contamination significantly affects the morphology of the corrosion product layer. In the  $\text{O}_2$ -free condition, a thick and porous iron sulfide layer is formed. This film contributes to the overall impedance as a porous electrode, leading to significant flattening towards a  $45^\circ$  line in the Nyquist plane. The huge specific surface of this film and its conductive nature gives rise to abnormally high double-layer capacitances, on the order of several tens of  $\text{mF}/\text{cm}^2$ . No such porous film behavior is seen with  $\text{O}_2$  contamination (500 ppb). Iron sulfide is still formed at the metal surface, though it appears to be far less adherent, and lacks any comparable porosity. The analysis of impedance data still estimates high capacitance values, but these are much lower compared against the  $\text{O}_2$ -free case, and indicative of a lower quantity of conductive and porous surface corrosion products. The corrosion rates of iron determined from the charge transfer resistance were found to agree well with traditional weight loss measurements, demonstrating the impedance model's validity and applicability.

Comparisons between corrosion densities and hydrogen permeation current densities were also calculated. While both values are similar in the absence of O<sub>2</sub> contamination, their difference increases continuously as O<sub>2</sub> – H<sub>2</sub>S reaction products build-up in the test solution. After 600 hours exposure, the corrosion current density is 6 times higher than the permeation current density, corresponding to permeation well below efficiency below 20%. This comparison suggests that the increase in corrosion rate is not only related to a less protective film, but also to the influence of additional reactions that result from the O<sub>2</sub> – H<sub>2</sub>S reactions. Here, we suspect that the electrochemical participation of thiosulfates leads to increasing corrosion rates with low hydrogen uptake.

### **Acknowledgements**

The authors kindly thank Alexandre Bonneau for the implementation of the experimental setup. Remy Mingant is also warmly acknowledged for his active participation in the analysis and modeling of impedance data. The contribution of IFPEN analysis department in the surface characterization and test solution analysis is also greatly acknowledged.

### **References**

- [1] T. Cassagne, G. Moulié, C. Duret-Thual, NACE Corrosion 2009, Atlanta, GA (USA), 22-26 March, 2009.
- [2] M.D. Deffo Ayagou, T.T. Mai Tran, B. Tribollet, J. Kittel, E. Sutter, N. Ferrando, C. Mendibide, C. Duret-Thual, *Electrochimica Acta* 282 (2018) 775–783.
- [3] J.L. Crolet, M. Pourbaix, A. Pourbaix, NACE Corrosion 1991, Cincinnati, OH (USA), 10-15 March, 1991.

- [4] Y. Song, A. Palencsar, G. Svenningsen, J. Kvarekval, T. Hemmingsen, Corrosion 68 (2012) 662–671.
- [5] L. Sow, J. Idrac, P. Mora, E. Font, Materials and Corrosion 66 (2015) 1245–1249.
- [6] M.D. Deffo Ayagou, J. Kittel, C. Mendibide, C. Duret Thual, k. belkhadiri, T.T. Mai Tran, E. Sutter, B. Tribollet, N. Ferrando, Corrosion 74 (2018) 1192–1202.
- [7] L. Choudhary, D.D. Macdonald, A. Alfantazi, Corrosion 71 (2015) 1147–1168.
- [8] NACE TM0177-2016: Laboratory testing of metals for resistance to sulfide stress cracking and stress corrosion cracking in H<sub>2</sub>S environments, Houston, TX, 2016.
- [9] M. Kappes, G.S. Frankel, N. Sridhar, R.M. Carranza, Journal of the Electrochemical Society 159 (2012) C195-C204.
- [10] H. Ma, X. Cheng, S. Chen, C. Wang, J. Zhang, H. Yang, Journal of Electroanalytical Chemistry 451 (1998) 11–17.
- [11] H.Y. Ma, X.L. Cheng, G.Q. Li, S.H. Chen, Z.L. Quan, S.Y. Zhao, L. Niu, Corrosion Science 42 (2000) 1669–1683.
- [12] C.I. Pearce, Reviews in Mineralogy and Geochemistry 61 (2006) 127–180.
- [13] F. Huang, P. Cheng, X.Y. Zhao, J. Liu, Q. Hu, Y.F. Cheng, Special issue on 1st International Conference on Hydrogen Storage, Embrittlement and Applications (Hy-SEA 2014), 26-30 October 2014, Rio de Janeiro, Brazil 42 (2017) 4561–4570.
- [14] M. Tjelta, J. Kvarekval, NACE Corrosion 2017 paper 9319, New Orleans, Louisiana, 22-26 March 2017.
- [15] R. de Levie, in: Paul Delahay (Ed.), Advances in Electrochemistry and Electrochemical Engineering: Volume 6 - Electrochemistry, Interscience publishers, 1967, pp. 330–397.

- [16] G.J. Brug, A.L.G. van den Eeden, M. Sluyters-Rehbach, J.H. Sluyters, *Journal of Electroanalytical Chemistry and Interfacial Electrochemistry* 176 (1984) 275–295.
- [17] B. Hirschorn, M.E. Orazem, B. Tribollet, V. Vivier, I. Frateur, M. Musiani, *Electrochimica Acta* 55 (2010) 6218–6227.
- [18] Y. Zheng, *Electrochemical mechanism and model of H<sub>2</sub>S corrosion of carbon steel*. PhD thesis, Athens, Ohio (USA), 2015.
- [19] J. Amri, J. Kvarekval, B. Malki, *Corrosion 2011*, Houston, TX (USA), 13-17 March, 2011.
- [20] N.A. Shvab, V.D. Litovchenko, L.M. Rudkovskaya, *Russ J Appl Chem* 80 (2007) 1852–1855.
- [21] O. Weres, L. Tsao, *Reaction of hydrogen sulfide with oxygen in the presence of sulfite: Report: Earth Sciences Division at Lawrence Berkeley Laboratory, University of California, University of California*, 1983.
- [22] L. Krayzelova, J. Bartacek, I. Díaz, D. Jeison, E.I.P. Volcke, P. Jenicek, *Rev Environ Sci Biotechnol* 14 (2015) 703–725.

Table 1: Component values related to the charge transfer loop obtained from the analysis of impedance data at various exposure times

	2 hours	47 hours	572 hours
$R_e$ ( $\Omega$ )	6.0	5.8	4.6
$Q_{dl}$ ( $mF s^{(\alpha-1)} cm^{-2}$ )	3.4	12.3	14.6
$\alpha_{dl}$	0.85	0.86	0.78
$C_{dl}$ ( $mF cm^{-2}$ )	2.8	12.6	14.9
$R_t$ ( $\Omega cm^2$ )	254	336	168
$J_{corr}$ ( $\mu A cm^{-2}$ )	68	52	103

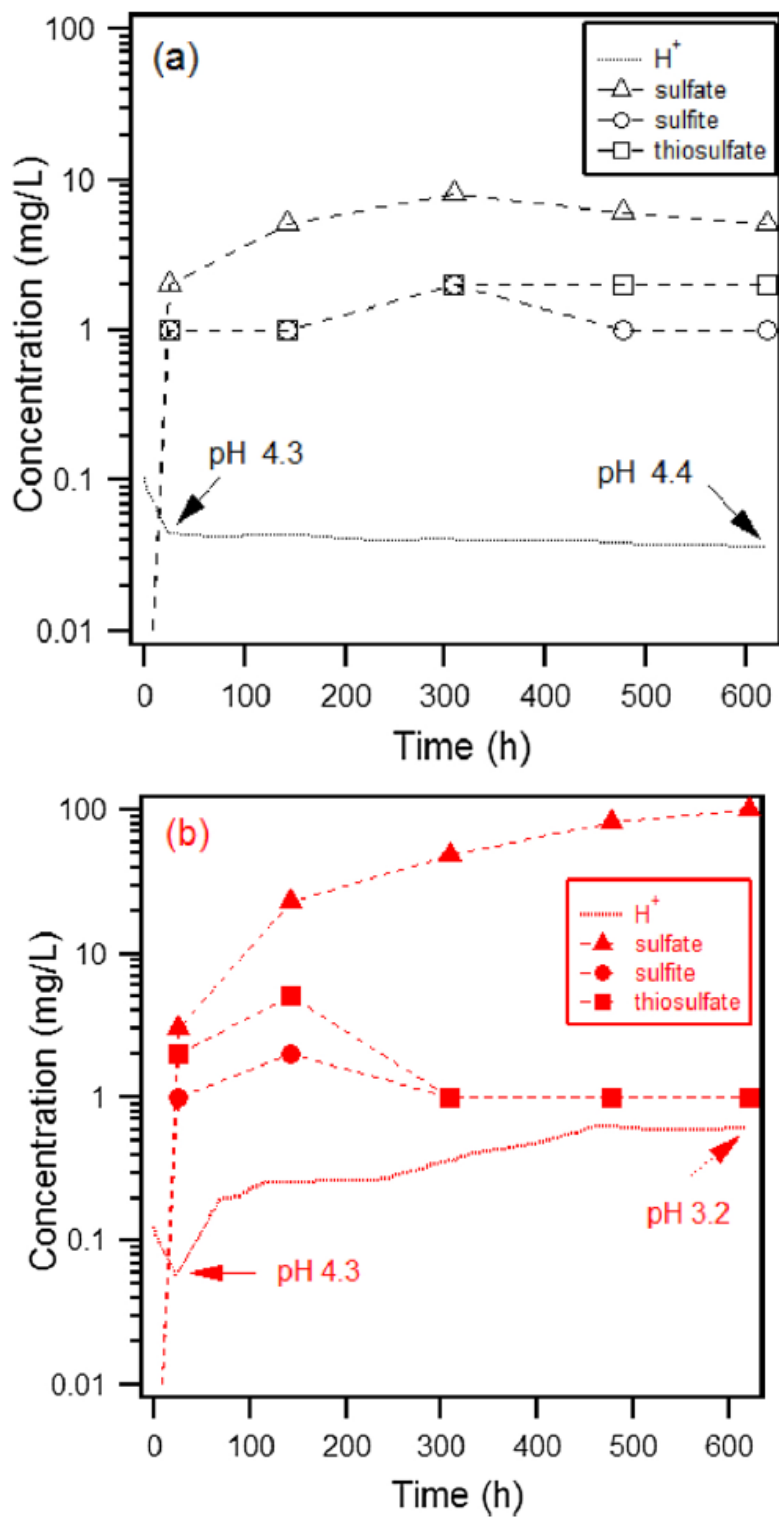


Fig. 1: The evolution of the bulk solution concentrations of  $H^+$  (from pH measurements) and primary aqueous  $H_2S-O_2$  reaction anion products of sulfites,

thiosulfates and sulfates as a function of time, in 35 g L<sup>-1</sup> NaCl solution saturated with 1 bar H<sub>2</sub>S at 24 °C, (a) without and (b) with oxygen pollution.

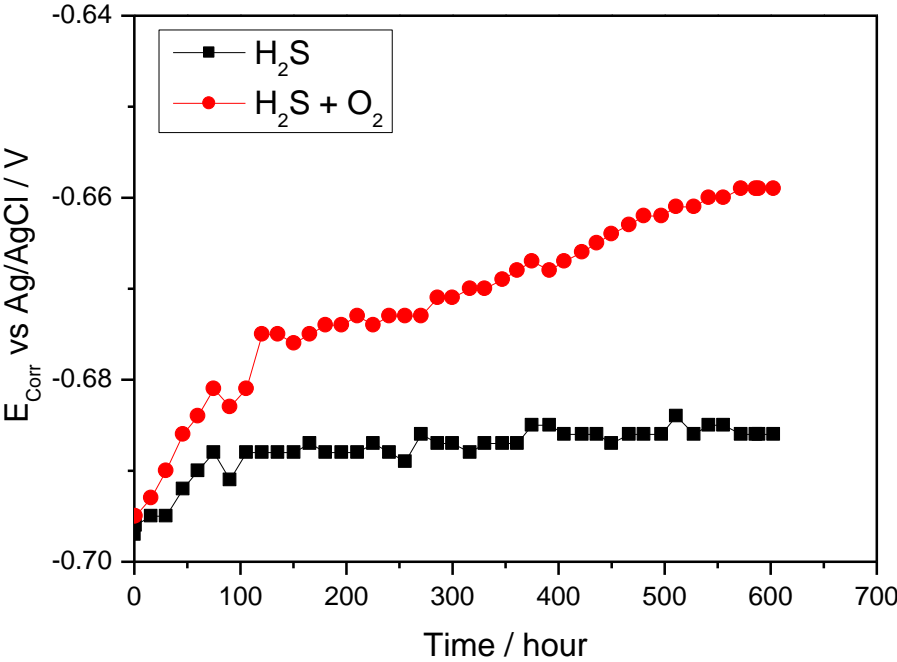


Fig. 2: The evolution of open circuit potentials of Fe in 35 g L<sup>-1</sup> NaCl solution saturated with 1 bar H<sub>2</sub>S at 24 °C, with (red) and without (black) oxygen pollution.

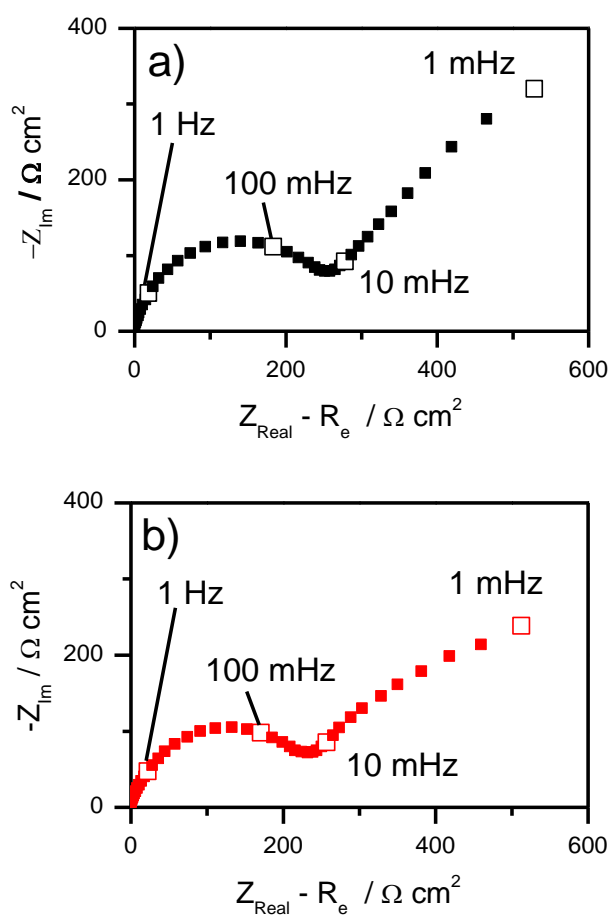


Fig. 3: Nyquist diagrams of pure iron measured after 2 hours exposure in  $35 \text{ g L}^{-1}$  NaCl saturated with 1 bar  $\text{H}_2\text{S}$  at  $24^\circ\text{C}$  for a)  $\text{O}_2$ -free and b)  $\text{O}_2$ -contaminated solutions.

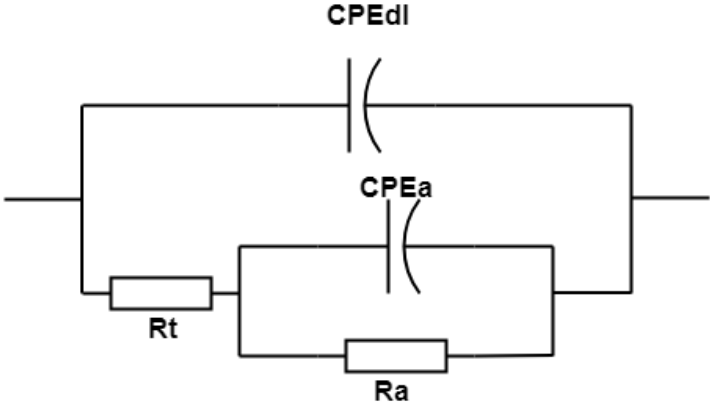


Fig. 4: Equivalent circuit for the corrosion of pure iron in H<sub>2</sub>S containing environment at short exposure times [10,11].

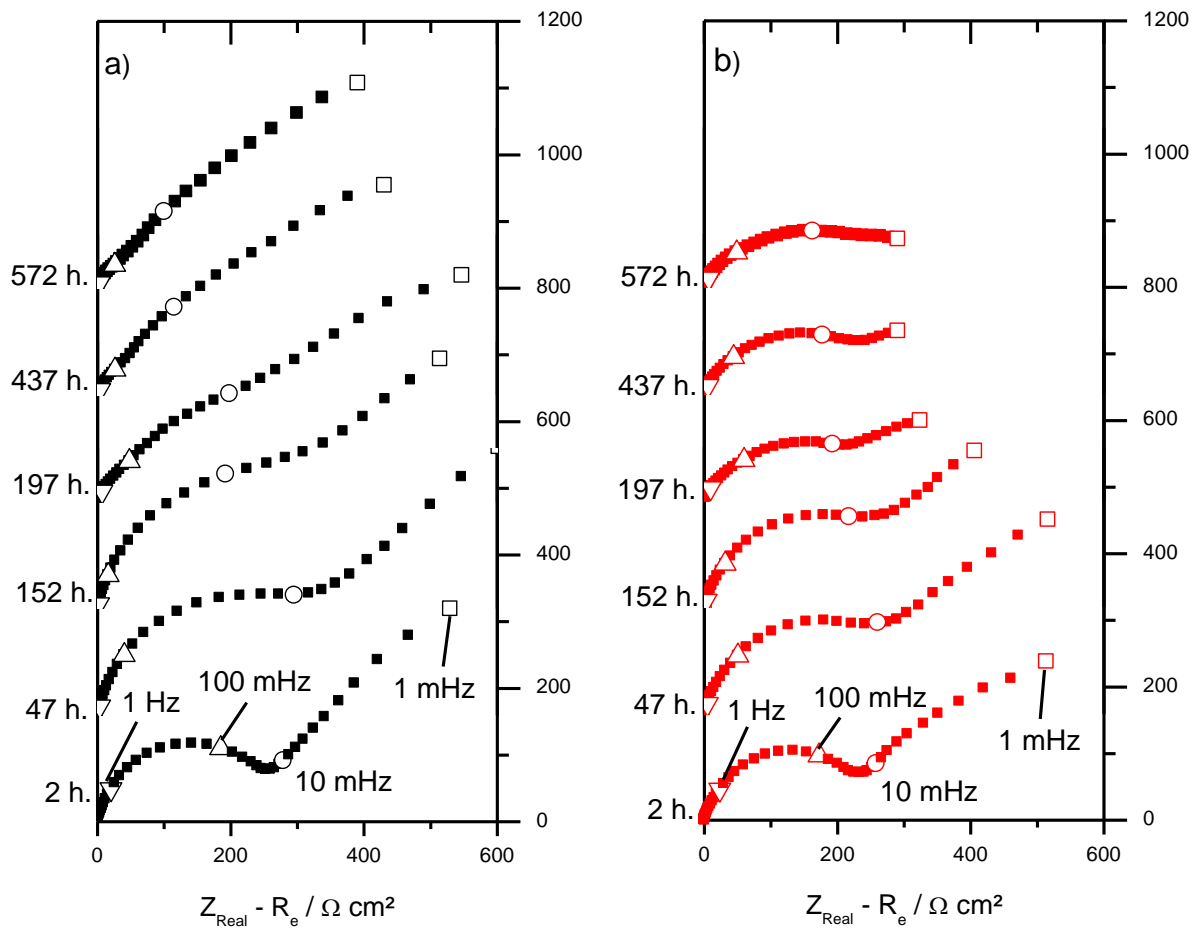


Fig. 5: Nyquist diagrams of pure iron exposed to 35 g L<sup>-1</sup> NaCl saturated with 1 bar H<sub>2</sub>S at 24°C for a) O<sub>2</sub>-free and b) O<sub>2</sub>-contaminated solutions at various exposure times (orthonormal representation with translation of Y-axis as exposure time increases).

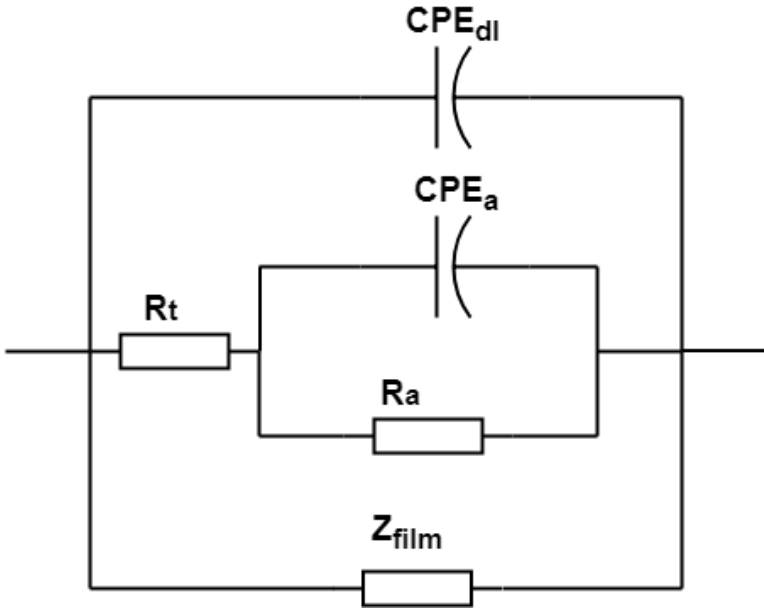


Fig. 6: Equivalent circuit for the corrosion of pure iron in H<sub>2</sub>S containing environment with the formation of a conductive and porous FeS layer [2].

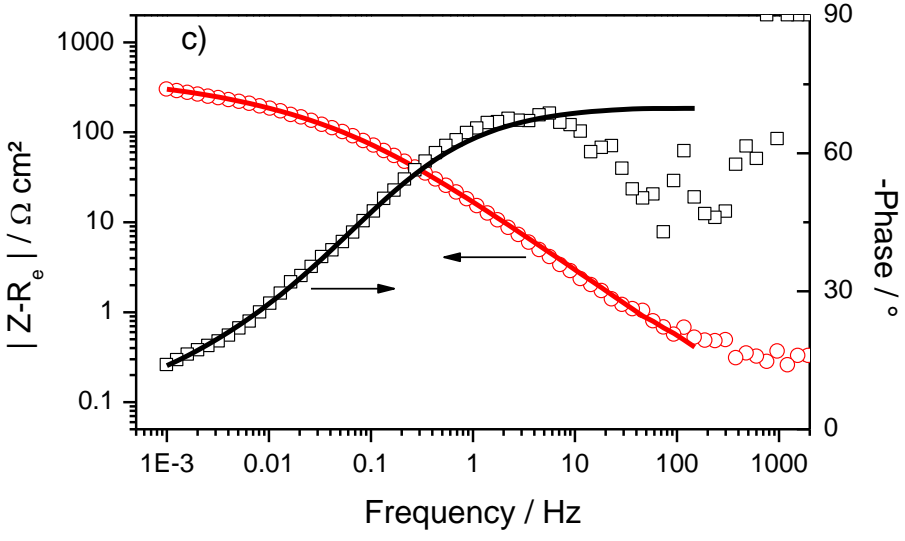
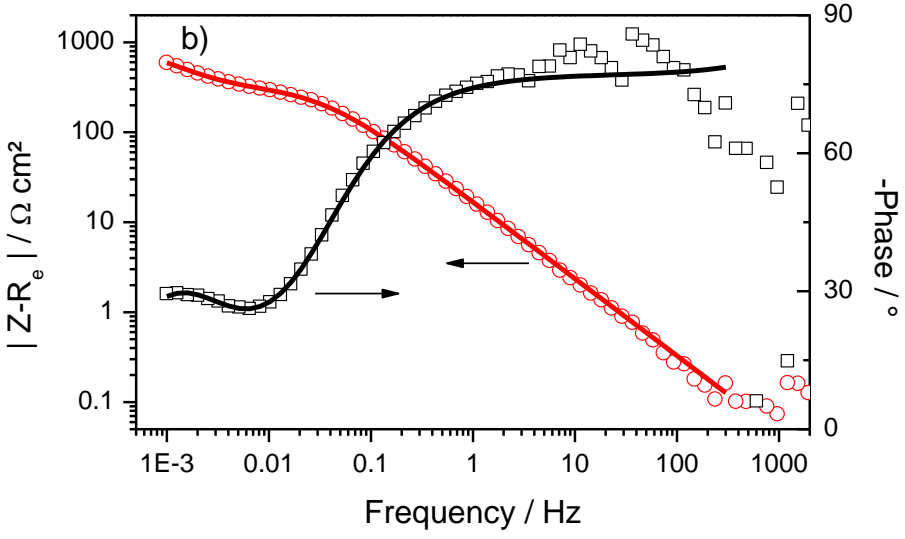
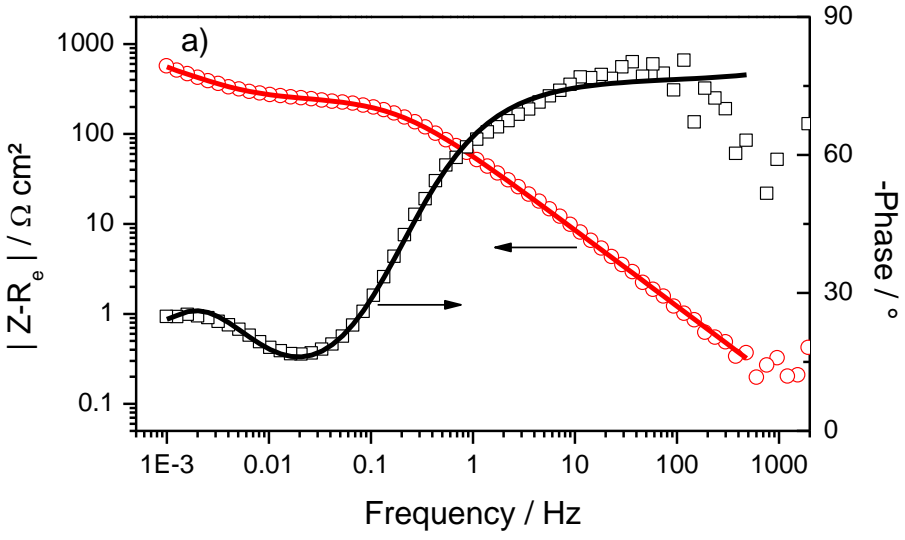


Fig. 7: Comparisons between experimental (open symbols) and fitted impedance (lines) measured after 2 h (a), 47 h (b) and 572 h (c) exposure in O<sub>2</sub>-contaminated solutions, using the equivalent circuit of Fig. 4.

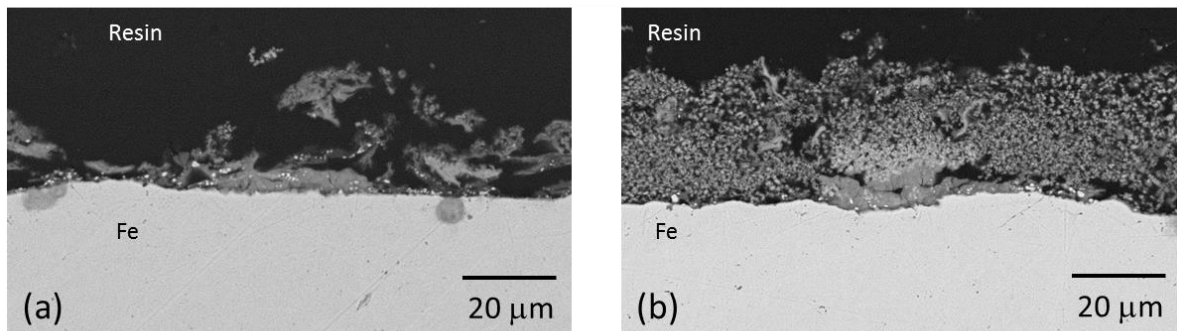


Fig. 8: Cross-sectional SEM images of pure iron after exposure to 35 g L<sup>-1</sup> NaCl saturated with 1 bar H<sub>2</sub>S at 24°C in a) O<sub>2</sub>-polluted and b) O<sub>2</sub>-free solution.

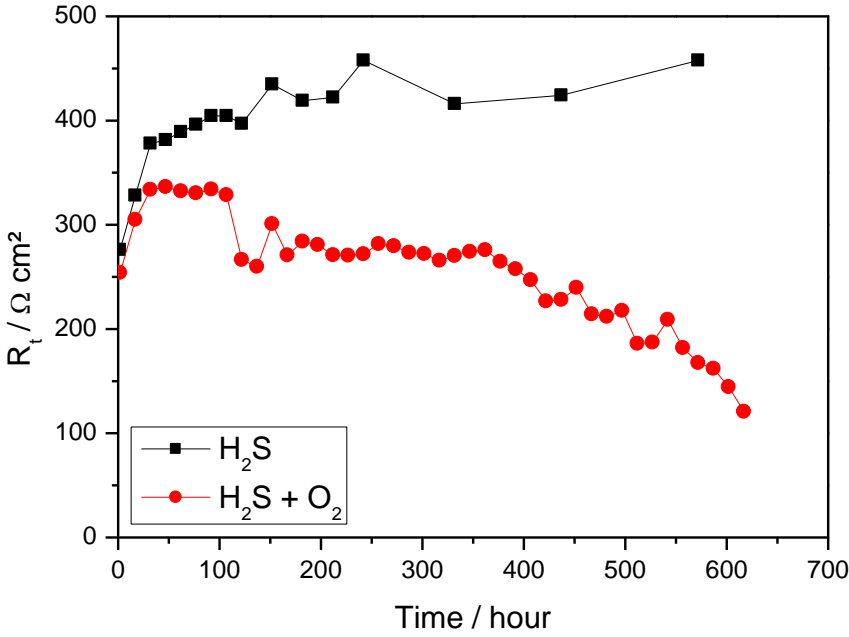


Fig. 9: Evolution of charge transfer resistance ( $R_t$  from EIS modeling) with and without oxygen contamination.

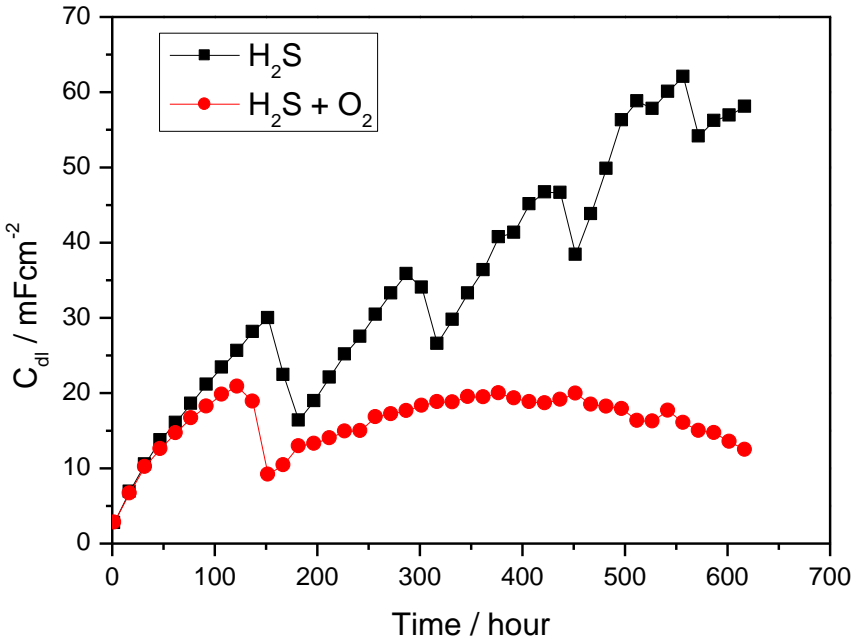


Fig. 10: Evolution of double layer capacitance ( $C_{dl}$  from EIS modeling) with and without oxygen contamination.

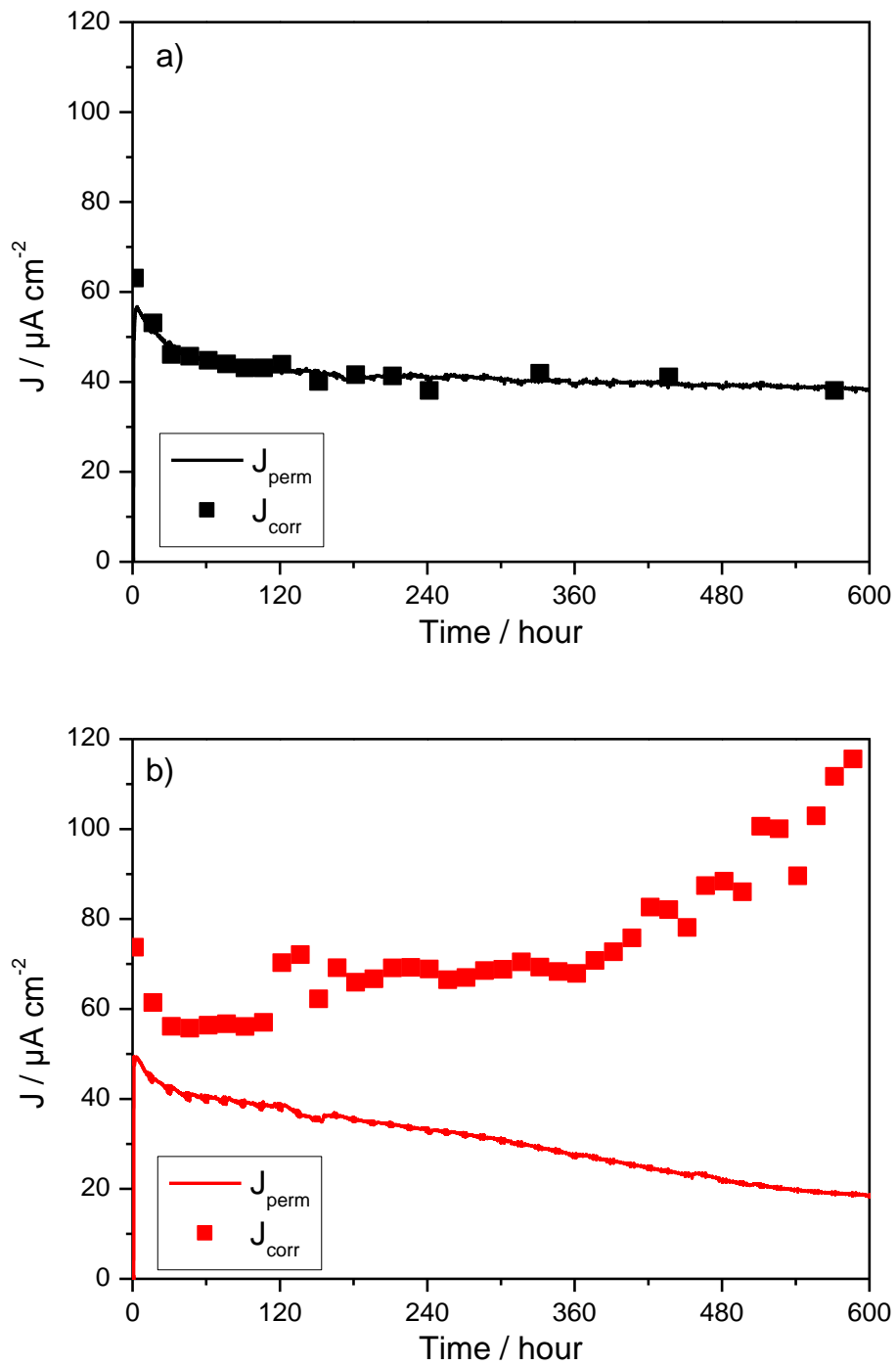


Fig. 11: Comparison of  $J_{perm}$  with  $J_{corr}$  determined from  $R_t$  values determined by EIS fitting for the tests without (a) and with (b)  $O_2$  contamination.